Optics Letters

# Microbubble-probe WGM resonators enable displacement measurements with high spatial resolution

Bonan Liu,[1,2] Shen Liu,[1,2,*] Qiang Zhang,[1,2] Guiqing Hong,[1,2] Changrui Liao,[1,2] Xizhen Xu,[1,2] Liwei Liu,[1] Junle Qu,[1] and Yiping Wang[1,2]

[1]Key Laboratory of Optoelectronic Devices and Systems of Ministry of Education/Guangdong Province, College of Physics and Optoelectronic Engineering, Shenzhen University, Shenzhen 518060, China
[2]Shenzhen Key Laboratory of Photonic Devices and Sensing Systems for Internet of Things, Guangdong and Hong Kong Joint Research Centre for Optical Fibre Sensors, Shenzhen University, Shenzhen 518060, China
*shenliu@szu.edu.cn

Received 19 December 2022; revised 3 March 2023; accepted 5 March 2023; posted 6 March 2023; published 30 March 2023

**A microbubble-probe whispering gallery mode resonator with high displacement resolution and spatial resolution for displacement sensing is proposed. The resonator consists of an air bubble and a probe. The probe has a diameter of ~5 μm that grants micron-level spatial resolution. Fabricated by a $CO_2$ laser machining platform, a universal quality factor of over $10^6$ is achieved. In displacement sensing, the sensor exhibits a displacement resolution of 74.83 pm and an estimated measurement span of 29.44 μm. As the first microbubble probe resonator for displacement measurement, the component shows advantages in performance, and exhibits a potential in sensing with high precision.**



https://doi.org/10.1364/OL.483285

Displacement sensing with high precision is of great significance in industrial measurement and control, high-precision processing, and intelligent manufacture. The measurement of strain, pressure, force, and vibration can also be realized through it [1–3]. Conventionally, displacement measurement is conducted through micro-electro-mechanical systems (MEMS). However, the electric nature restrains the performance and practicality of MEMS components, especially under complex environments. The development of optical fiber sensors brings novel solution for displacement sensing.

Several kinds of optical fiber-based components have been used for displacement sensing, including Fabry–Perot interferometer (FPI) [4,5], Mach–Zehnder interferometer (MZI) [6–8], surface plasmon resonance (SPR)-based sensors [9,10], multimode fiber interferometer (MMI) [11], and fiber gratings [12,13]. Song *et al*. developed a liquid-crystal-based FPI displacement sensor and achieved a wide dynamic range of 0.9 mm with a resolution of 6.7 nm [14]. Tian *et al*. proposed a displacement sensor based on an MMI [11]. The sensor achieved a sensitivity of 36 pm/μm and a dynamic range of 100 μm. A fiber Bragg grating sensor is reported by Tao, Dong, and Lai in 2016 [15]. The displacement sensor exhibits a wide measurement range of 3 mm but with a sensitivity of 0.57 pm/μm. However, the performance of these components is not sufficient for high-precision measurement. Especially for micro objects, components with high spatial resolution are required.

The whispering gallery mode (WGM) resonator is known for its high performance in measurement. Due to its inherent advantages of high-quality (Q) factor, small mode volume, and high optical energy density, it exhibits predominant sensitivity and resolution in sensing application. Various applications including biomedical sensing [16–18], magnetic field measurement [19], and ultrasound sensing [20] have been performed on the WGM platform. Micro force detection has been also realized on probe-based resonators [21,22]. However, it is still challenging to achieve high-Q factor. The same as a microdisk, microtoroid, and microsphere, a microbubble is a typical category of WGM cavities. With the hollow cavity and micro channel endowed by its particular structure, a microbubble WGM resonator is advantageous in microfluid measurement [23] and strain-related measurement [24–28].

In our study, a silica microbubble probe resonator (MPR) for displacement sensing is proposed. The MPR exhibits high displacement and space resolution and was fabricated with a silica capillary (SC) by $CO_2$ laser machining. Having a probe on the tip of the microbubble, the component shows a micron-level spatial resolution allowing the measurement on micro objects. Samples with the different diameter were demonstrated, and a universal Q factor of over $10^6$ is achieved. The resonators were used for a displacement sensing test. An MPR with a diameter of 86 μm exhibited a sensitivity of 51.89 pm/μm with a linearity of 98.38%. The displacement resolution was determined to be 74.83 pm. Having a free spectral range (FSR) of ~1.53 nm, the measurement span of the sensor is estimated to be 29.44 μm.

The machining setup is essentially the same as that shown in [29]. The two translation stages can be controlled to move linearly with a minimum step of 1 μm. The SC selected herein has an inner diameter of 250 μm and an external diameter of 350 μm.

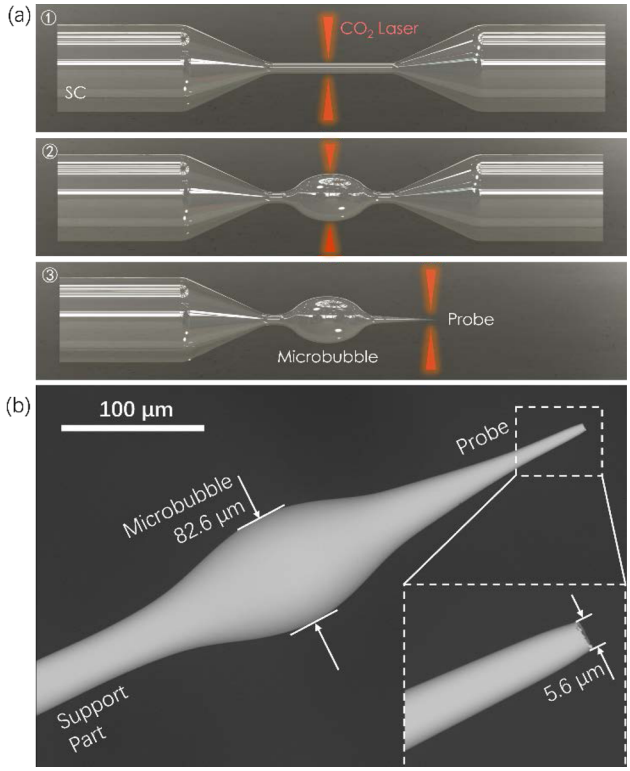


**Fig. 1.** (a) Schematic of the major fabrication steps. (b) Structure SEM images of the microbubble probe. The component contains a support part, a microbubble, and a probe.

As shown in Fig. 1(a), the fabrication of the microbubble probe (MP) mainly includes three steps. Initially, an SC was mounted on two translation stages. After the SC was melted by the laser spots, the two stages were controlled to move oppositely by which a waist is formed in the middle. By pressurizing the SC, the inner air pressure became larger than the external so that the waist can be expanded to a bubble under the heating of laser spots. The inner pressure used is approximately 300 kPa. Lastly, one side of the waist was moved to the middle. By heating and pulling oppositely, the waist broke and formed a probe. The inner pressure can be 300 kPa–1 MPa, while a small pressure is preferable since it helps the careful control of the bubble expansion. The length of the probe is directly related to the power of the $CO_2$ laser, e.g., a short probe can be easily obtained with a relatively small power of hundreds of milliwatts.

The structure of a typical MP component obtained is illustrated in Fig. 1(b) by the scanning electron microscopy (SEM) images. The diameter of the microbubble and the probe tip is 82.6 μm and 5.6 μm, respectively. The sensitivity of the sensor highly depends on the shape of the microbubble. Including the size, diameter, and wall thickness, factors have been discussed in previous studies [24,30]. Obviously, microbubbles with a thin wall can achieve high sensitivity but with a price of narrow measurement range due to its low mechanical strength. This is because the maximum force sustainable is linked to the wall thickness and the bubble diameter [22].

To investigate the effect brought by the structure, two example MPs obtained are demonstrated here with their microscopy images and spectra measured, as illustrated in Fig. 2. The MPR shown in Fig. 2(a) has a diameter of 114 μm and exhibits a full width at half maximum (FWHM) in spectrum of 76.5 MHz

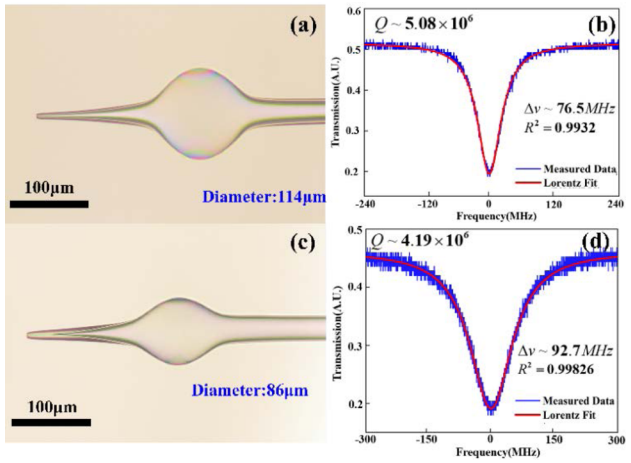


**Fig. 2.** (a) Microbubble probe with a diameter of 114 μm and (b) its strongest resonance dip measured. (c) Microbubble probe with a diameter of 86 μm and (d) its strongest resonance dip measured.

which indicates a Q factor of $5.08\times10^6$. That shown in Fig. 2(c) has a diameter of 86 μm and has a FWHM of 92.7 MHz, yielding a Q factor of $4.19\times10^6$. Their resonance dip follows a Lorentz fit and exhibits a universal Q factor level of $\sim10^6$. Clearly, the difference in size leads to the difference in the spectrum.

To obtain the MPR, a tapered fiber is required to couple the light into the microbubble cavity. The tapered fiber has a waist diameter of ~2 μm and a transmission loss of ~0.5 dB. Forming WGM resonance in the equatorial plane, any changes in the cavity diameter can lead to the shift of resonance dips [22]. The WGM resonance and the displacement test were measured using the setup illustrated in Fig. 3. A metal board on a translation stage (Q545.140, PI) was set in front of the probe. The stage has a minimum incremental motion of 6 nm and a sensing resolution of 1 nm for feedback. After the probe touches the board, the displacement brought by the board can be received by the probe. The probe introduces such displacement into the microbubble, which leads to a compression on the microbubble. The compression of the microbubble brings a variation in equatorial diameter, which changes the resonance condition of the WGM therein. A dip drift can be observed consequently. During the process, the microbubble compresses dominantly while the probe and the support parts deform minorly. This means that the component can bear more displacement than the limit endurance of the microbubble. It was observed that a microbubble with a diameter of ~80 burst when a displacement of 90 μm was applied. When the microbubble is close to bursting, the spectrum distorted due to the nonlinear deformation and coupling change.

Figure 4(a) shows the spectrum evolution of an MPR with a microbubble diameter of 52 μm. As the displacement increased from 0 to 700 nm, the dip of interest underwent a wavelength redshift of 19.67 pm, which shows a sensitivity of 28.13 pm/μm with a good linearity of 99.97%. The Q factor is calculated to be $\sim1.27\times10^6$. Figure 4(b) gives the comparison of two MPR test results. An MPR with larger microbubble diameter of 86 μm exhibits a higher displacement sensitivity of 51.89 pm/μm with a linearity of 98.38%. It can be observed that the sensitivity can be improved by increasing the microbubble diameter.

The detection limit (DL), indicating the minimum displacement measurable, the displacement resolution herein, can be

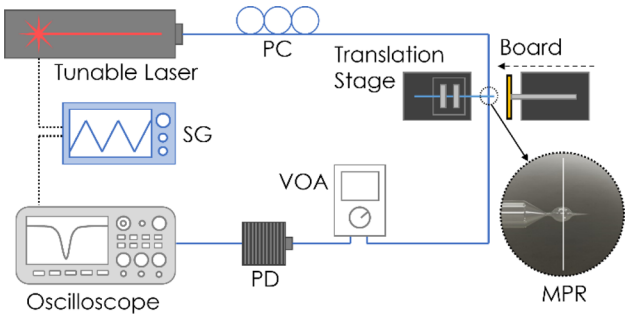


**Fig. 3.** Schematic of the displacement sensing setup.

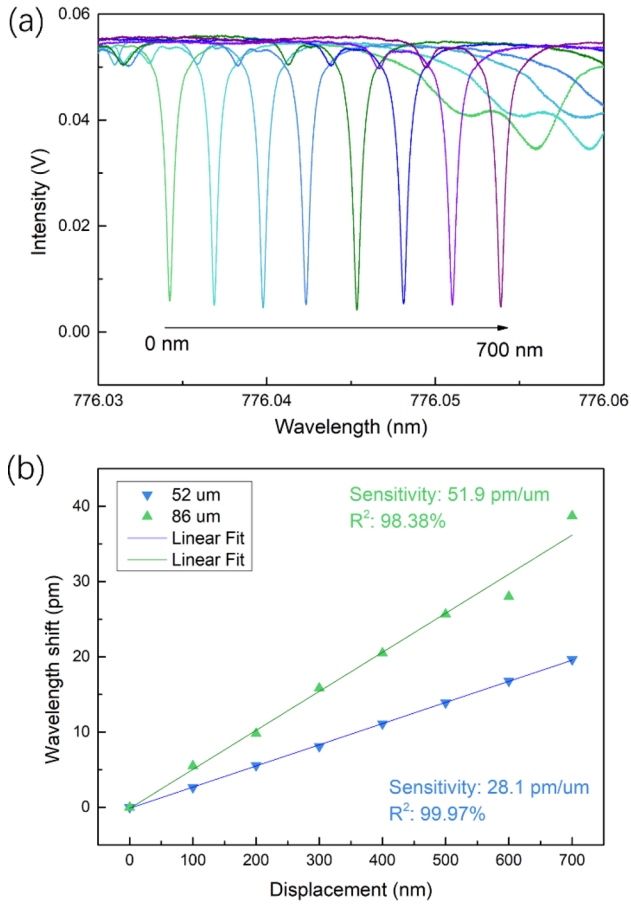


**Fig. 4.** (a) Spectral evolution versus displacement of the microbubble with a diameter of 52 μm. (b) Test results for two microbubbles with a diameter of 52 μm (in blue) and 86 μm (in green).

determined as [31]

$$\mathrm{DL} = \frac{R}{S}, \tag{1}$$

where $R$ is the sensor resolution indicating the minimum spectral shift that can be measured accurately and $S$ represents the sensitivity. The sensor resolution can be known through $\boldsymbol{R} \approx 3\boldsymbol{\sigma}$, where [31]

$$\sigma \approx \frac{\Delta\lambda}{4.5(\mathrm{SNR}^{0.25})}, \tag{2}$$

where Δλ is the FWHM of the resonance dip that relates to the Q factor. SNR is the signal to noise ratio. To evaluate the exact performance of the MPR, a typical value of 60 dB is selected for calculation [31].

**Table 1. Microbubble DL Calculation Parameters**

| | MPR 1 | MPR 2 |
|---|---|---|
| Q factor | $1.27 \times 10^6$ | $4.19 \times 10^6$ |
| FWHM (pm) | 0.61 | 0.18 |
| σ (nm) | $4.28 \times 10^{-6}$ | $1.29 \times 10^{-6}$ |
| Sensor resolution (nm) | $1.28 \times 10^{-5}$ | $3.88 \times 10^{-6}$ |
| Sensitivity (pm/μm) | 28.13 | 51.89 |
| DL (pm) | 457.16 | 74.83 |

Combining with the results acquired, the DL of the device can be found to be 74.83 pm. The FSR is calculated to be 1.53 nm. Therefore, the measurement range is calculated to be 0 to 29.44 μm. The calculation parameters are listed in Table 1.

In conclusion, a novel microbubble probe based WGM resonator with high displacement and spatial resolution is proposed. Fabricated by $CO_2$ laser micro machining, the microbubble cavities achieve a universal Q factor level of ~$10^6$. Benefiting from the micron-level spatial resolution of the probe, measurements can be conducted on micro objects. One of the resonators was tested with displacement sensing, and shows a sensitivity of 51.89 pm/μm and a linearity of 98.38%. Silica microbubbles possess good mechanical strength and resistance against extreme conditions but at the price of a relatively lower sensitivity compared to other materials with low Young's modulus. The sensitivity of the sensor can be further improved by optimizing the geometry of the microbubble such as diameter, wall thickness, and axial size. The minimum displacement resolution is calculated to be 74.83 pm while the measurement span is estimated as 29.44 μm. This resonator sensor with high displacement resolution and spatial resolution exhibits a potential in high-precision displacement-related measurements.

**Funding.** National Natural Science Foundation of China (62175165, U1913212); Basic and Applied Basic Research Foundation of Guangdong Province (2021A1515011834); Shenzhen Science and Technology Innovation Program (JCYJ20210324120403009, RCBS20200714114922296).

**Disclosures.** The authors declare no conflicts of interest.

**Data availability.** Data underlying the results presented in this paper are not publicly available at this time but may be obtained from the authors upon reasonable request.

## REFERENCES

1. F. Khoshnoud and C. W. de Silva, IEEE Instrum. Meas. Mag. **15**, 14 (2012).
2. C. Trigona, B. Ando, and S. Baglio, IEEE Trans. Instrum. Meas. **63**, 702 (2014).
3. T. Iwasaki, T. Takeshita, Y. Arinaga, K. Uemura, H. Ando, S. Takeuchi, M. Furue, E. Higurashi, and R. Sawada, Sens. Actuators, A **221**, 1 (2015).
4. M. Gutierrez-Rivera, D. Jauregui-Vazquez, D. F. Garcia-Mina, J. M. Sierra-Hernandez, J. M. Estudillo-Ayala, M. Almanee, and R. Rojas-Laguna, IEEE Sens. J. **20**, 4719 (2020).
5. X. Yin, Y. Shen, W. Wang, Z. Shao, and Q. Rong, IEEE Sens. J. **19**, 9249 (2019).
6. Y. Liu, W. Wang, and Y. Li, Opt. Eng. **56**, 027107 (2017).
7. H. Luo, X. Li, W. Zou, X. Li, Z. Hong, and J. Chen, IEEE Photonics J. **4**, 772 (2012).
8. L. Zhao, H. Li, Y. Song, M. Dong, and L. Zhu, Photonics Sens. **9**, 97 (2019).
9. C. Liu, P. Wu, Y. Wei, B. Li, Y. Su, X. Zhao, R. Wang, and L. Li, Sens. Actuators, A **335**, 113360 (2022).

10. Z. Zhu, L. Liu, Z. Liu, Y. Zhang, and Y. Zhang, Opt. Lett. **42**, 1982 (2017).
11. K. Tian, G. Farrell, X. Wang, E. Lewis, and P. Wang, Appl. Opt. **57**, 9662 (2018).
12. Q. Wang, M. Guo, and Y. Zhao, IEEE Trans. Instrum. Meas. **66**, 122 (2017).
13. L. Qi, C. Zhao, Y. Wang, J. Kang, Z. Zhang, and S. Jin, Opt. Express **21**, 3193 (2013).
14. B. Song, J. Hu, C. Xia, H. Zhang, Y. Lu, W. Sun, and Y. Liu, Appl. Opt. **58**, 410 (2019).
15. S. Tao, X. Dong, and B. Lai, Opt. Commun. **372**, 44 (2016).
16. Y. N. Zhang, T. Zhou, B. Han, A. Zhang, and Y. Zhao, Nanoscale **10**, 13832 (2018).
17. L. Fu, Q. Lu, X. Liu, X. Chen, X. Wu, and S. Xie, Talanta **213**, 120815 (2020).
18. P. Niu, J. Jiang, K. Liu, S. Wang, J. Jing, T. Xu, T. Wang, Y. Liu, and T. Liu, Biosens. Bioelectron. **208**, 114238 (2022).
19. B.-B. Li, G. Brawley, H. Greenall, S. Forstner, E. Sheridan, H. Rubinsztein-Dunlop, and W. P. Bowen, Photonics Res. **8**, 1064 (2020).
20. S. Basiri-Esfahani, A. Armin, S. Forstner, and W. P. Bowen, Nat. Commun. **10**, 132 (2019).
21. J. Chae, S. An, G. Ramer, V. Stavila, G. Holland, Y. Yoon, A. A. Talin, M. Allendorf, V. A. Aksyuk, and A. Centrone, Nano Lett. **17**, 5587 (2017).
22. M. Sumetsky, Y. Dulashko, and R. S. Windeler, Opt. Lett. **35**, 1866 (2010).
23. K. H. Kim, G. Bahl, W. Lee, J. Liu, M. Tomes, X. Fan, and T. Carmon, Light: Sci. Appl. **2**, e110 (2013).
24. S. Liu, Z. Sun, L. Zhang, C. Fu, Y. Liu, C. Liao, J. He, Z. Bai, Y. Wang, and Y. Wang, Opt. Lett. **43**, 4077 (2018).
25. C. Sun, Y. Liu, Y. Li, and S. Qu, Opt. Express **30**, 8750 (2022).
26. R. Madugani, Y. Yang, V. H. Le, J. M. Ward, and S. Nic Chormaic, IEEE Photonics Technol. Lett. **28**, 1134 (2016).
27. Y. Guo, H. Su, Y. Zhang, K. Qi, F. Zhu, C. Yu, and G. Yi, Opt. Laser Technol. **139**, 106762 (2021).
28. R. Henze, T. Seifert, J. Ward, and O. Benson, Opt. Lett. **36**, 4536 (2011).
29. Y. Yang, S. Saurabh, J. M. Ward, and S. Nic Chormaic, Opt. Express **24**, 294 (2016).
30. B. Xu, M. Chen, K. Yang, Y. Guo, D. N. Wang, and C. L. Zhao, Opt. Lett. **46**, 1983 (2021).
31. I. M. White and X. Fan, Opt. Express **16**, 1020 (2008).